Article (refereed)

Doyle, Timothy E.; Tew, Adam T.; Jain, Rahul; **Robinson, David A.**. 2009 Effects of aggregation on the permittivity of random media containing monodisperse spheres. *Journal of Applied Physics*, 106 (11), 114104. 10.1063/1.3264722

Effects of aggregation on the permittivity of random media containing monodisperse spheres

Timothy E. Doyle

Department of Physics, Utah State University, Logan, Utah 84322-4415

Adam T. Tew

Department of Geophysics, Stanford University, Stanford, California 94305-2215

Rahul Jain

Department of Physics, Utah State University, Logan, Utah 84322-4415

David A. Robinson

Centre for Ecology and Hydrology, Environment Centre Wales, Bangor, UK

Abstract

Numerical simulations were used to calculate the effective permittivities of three-dimensional random particle suspensions containing up to 2440 particles and exhibiting two types of particle aggregation. The particles were modeled as 200-μm spheres that were aggregated into either large spherical clusters or into foam-type microstructures with large spherical voids. Multiple scattering of 0.01-10.0 GHz electromagnetic fields was simulated using a first-principles iterative multipole approach with matrix and particle permittivities of 1.0 and 8.5, respectively. The computational results showed both significant and highly significant trends. Aggregation

into spherical clusters decreased the effective permittivity by up to 3.2 ± 0.2%, whereas aggregation into foam-type microstructures increased the effective permittivity by up to 3.0 ± 1.6%. The effective permittivity trends exhibited little change with frequency. These results were compared to effective medium approximations that predicted higher permittivities than those from the simulations and showed opposite trends for cluster aggregation. Three theories are proposed to explain the simulation results. The first theory invokes a waveguide-like mechanism. The simulations indicate that the wave fields propagate more through the continuous paths of greater or lesser particle density created by aggregation, rather than through the isolated particle clusters or large voids. This quasi-continuous phase, or quasi-matrix, therefore behaves like a random waveguide structure in the material. A second theory is proposed where the quasi-continuous phase governs the behavior of the system by a percolation- like process. In this theory, the multipole interactions are modeled as the percolation of virtual charges tunneling from one particle to another. A third mechanism for the permittivity changes is also proposed involving collective polarization effects associated with the particle clusters or large voids. The simulation results challenge the general applicability of the quasistatic limit for heterogeneous media by showing how microstructural changes much smaller than the electromagnetic wavelength can alter the effective permittivity by a statistically significant degree. The results also provide a quantitative indication of the effects of aggregation and hierarchical microstructures on the electromagnetic properties of random media, and have application to the remote and *in situ* sensing of soils, the rational design and nondestructive evaluation of composites, and the study of biological tissues and other random materials.

I. INTRODUCTION

Determining the effective electromagnetic (EM) properties of suspensions, dispersions, and other heterogeneous materials has been a goal in physics for over 150 years since the early studies of Faraday, Maxwell, and Rayleigh.[1,2,3] This goal is important for a fundamental understanding of wave propagation in random multiphase media, but has remained elusive due to strong multiple scattering between phases with high property contrasts. Spherical particle suspensions have also been important as model systems for understanding the physics of granular media, amorphous materials, percolation phenomena, and phase transitions,[4,5] and a thorough understanding of spherical systems serves as a platform for developing more sophisticated models for more complex geometries. Additionally, how microstructural changes in materials influence their physical properties is a central question in condensed matter physics, as is the role of the wavelength of the incident field in resolving microstructural changes at vastly smaller length scales.

Relating effective properties to material microstructures at multiple scales has received less attention due to the complexities and computing power needed to model such systems, yet this area of research has many practical applications for remote and *in situ* material sensing methods, materials engineering, and bioengineering. In particular, there is growing interest in the dielectric behavior of soils and sediments in the earth sciences.[6] Dielectric methods have become a standard approach for determining soil water content from both *in situ* measurements and remote sensing.[7,8] Recently, the use of ground penetrating radar (GPR) has been applied to determining earth structure.[9] However, researchers are increasingly recognizing that the soil or sediment microstructure plays an important role in determining the effective dielectric response.[10,11] For example, particle aggregation has recently been shown to affect the dielectric

response of soils, which is important as soils vary in their degree of aggregation. Consequently, studies suggest aggregation affects the EM measurement of soil water content.[12,13]

In materials science, vigorous research is being pursued to design composites with new or enhanced properties. Such composites include particle-, fiber-, and whisker-reinforced polymers and ceramics; photonic crystals; metamaterials; piezoelectric polymer foams and polymer-ceramic composites; multifunctional materials combining structural, sensing, actuating, and self-repair capabilities; and nanoscale electronic materials such as magnetoelectric nanocomposites, carbon nanotube composites, and spintronic materials.[14-16] Having accurate models for the effective permittivity of random media is also critical for the nondestructive evaluation or process monitoring of composites and mixtures using capacitance measurements, impedance spectroscopy, and microwave methods.[17,18]

In biological media, dielectric spectroscopy has been used to measure the effective permittivity of cell suspensions and tissues to characterize properties such as yeast cell morphology and cell division.[19,20] Modeling the EM field at both the cellular level and at the macroscopic (effective field) level in tissues also has important applications in the assessment of the biological safety of EM fields from sources such as cell phones and power lines, in the determination of enzyme reaction rates and gene expression in cells exposed to EM fields, in the detection of breast and liver cancer with microwaves, and in radio-frequency and microwave ablation therapies for tumors.[21-24]

Particle aggregation forms multiscale structures that include mesoscale aggregates or voids in addition to the microscale particles. Thus far the effective properties of these types of materials have yet to be modeled adequately, especially in terms of frequency domain response. Many analytical formulas have been developed to predict the effective properties of two-phase

mixtures comprised of a discontinuous inclusion or particle phase embedded in a continuous matrix phase.[4,25-30] Formulas have been derived to model not only isotropically distributed, spherical particles but also ellipsoidal particles, layered particles, anisotropic mixtures, and chiral mixtures.[28,29] These approximations may not adequately model the affects of aggregation and hierarchical microstructures in a material since the field interactions are statistically averaged. In contrast, a numerical approach can calculate the multiple scattering between particles for a specific material microstructure, thereby providing effective properties based on a detailed microscopic description of the medium and EM field interactions.

Conventional numerical approaches such as the finite element (FE) and finite-difference time-domain (FDTD) methods have provided benchmark results for the modeling of random media.[30] These methods are currently limited to simple heterogeneous materials, however, and are too computationally intensive for modeling large, complex systems such as aggregate and hierarchical microstructures. Since FE and FDTD calculations are challenging even for uniformly dispersed mixtures, several methods have been devised to reduce the computational burden. These include the use of small systems, periodic boundary conditions, and two- dimensional (2D) models in place of three-dimensional (3D) models. Several FE models have calculated the permittivity of composites and mixtures by applying periodic boundary conditions to a square or cubic unit cell containing a small number (1-134) of circular,[31-35] spherical,[31] or prismatic inclusions.[16] FE calculations have also been combined with the method of boundary-integral equations (BIE) to simulate single inclusions of various shapes, including ellipsoids and cylinders, in 2D and 3D unit cells.[14] Similarly, the FDTD method has been used to model 2D mixtures containing up to 265 inclusions (1.0 inclusion volume fraction),[36,37] and to model the EM properties of biological tissues using periodic stacks of 30-100 spherical cells;[21] Other

approaches used to model the permittivity of random media include the transmission line matrix (TLM) method, which was applied to 2D simulations of 64-127 inclusions in a square periodic unit cell (0.5-1.0 inclusion volume fraction),[38] and the lattice Boltzmann method, which used 2D simulations to model fluid aggregation (wetting) in multiphase microporous materials.[39]

Multipole expansion methods are efficient tools for modeling field interactions in arbitrary 3D configurations of spherical particles since the fields for a particle can be defined by a relatively small number of expansion coefficients rather than a large number of grid values as required for approaches such as the FE method. Multipole methods include the iterative multipole approach, the fast multipole method, the *T*-matrix method, and other matrix methods.[40]
Matrix methods have been limited to the modeling of only a few hundred random particles,[41] although one approach constructed larger quasi-random structures by incorporating these particles into a periodic cell.[42] Recently, an iterative multipole approach was developed that modeled the permittivity of up to 3600 monodisperse glass spheres in air.[43] The spheres were configured in either ordered lattices or random microstructures, and with particle volume fractions of 0.025-0.60.[43]

This article reports on the use of the iterative multipole approach to study the effects of particle aggregation, multi-level porosity, and hierarchical microstructures on the dielectric permittivity of random two-phase mixtures containing monodisperse spheres. Various levels of aggregation were simulated where the aggregation formed either large spherical clusters or large spherical voids. Additionally, for each level of aggregation five different microstructural variations were modeled where the particle and cluster/void locations were changed in order to determine the standard deviation of the results. Finally, the numerical results were compared to analytical approximations derived from effective-medium formulas.

II. METHODS

A. Numerical algorithm

The numerical model used an iterative multipole approach that directly simulates multiple scattering and calculates the dielectric properties of 3D, arbitrary packings of spherical particles.[43] Simulations were performed on particle packs containing up to 2440 particles to assess the effects of aggregation (clustering) and foaming (void formation) on random microstructures. The spherical particles were configured in a cylinder of fixed volume with the EM field propagating parallel to the cylinder's axis (*z* direction) and with the electric field vector perpendicular to the axis (*x* direction). The particles were modeled with a diameter of 200 μm and a permittivity of 8.5 to represent a fine-grained calcareous sediment or soil.[44] The matrix had a permittivity of 1.0 to represent either air or vacuum. The particle packs were constructed by Monte Carlo and reduced dimension algorithms for random particle packing.[45-47] Aggregate microstructures with various levels of aggregation (local particle volume fractions) were generated by defining randomly distributed spherical regions in the pack and altering the particle volume fraction within the region. Five different structures were simulated for each level of aggregation to determine the average and standard deviation of the effective permittivity values. The structures differed in specific particle and cluster/void locations.

The details of the iterative multipole approach have been previously reported for both EM and elastic wave scattering.[43,48] The EM fields of the spherical particles were modeled with vector multipole functions derived from the Maxwell equations for a macroscopic dielectric medium with no free charges. These functions are solutions to the vector Helmholtz equations in spherical coordinates, and are also known as vector spherical wave functions:

$$\mathbf{V} = \sum_{n=0}^{\infty} \sum_{m=-n}^{+n} \left(i\sqrt{\frac{n+1}{2n+1}}\, z_{n-1}(kr)\mathbf{Y}^{n-1}_{nm}(\theta,\phi) - i\sqrt{\frac{n}{2n+1}}\, z_{n+1}(kr)\mathbf{Y}^{n+1}_{nm}(\theta,\phi) \right), \tag{1}$$

$$\mathbf{W} = \sum_{n=0}^{\infty} \sum_{m=-n}^{+n} z_n(kr)\mathbf{Y}^{n}_{nm}(\theta,\phi). \tag{2}$$

where $\mathbf{Y}^{l}_{nm}(\theta,\phi)$ is a pure-orbital vector spherical harmonic and $z_n(kr)$ is a radial function representing a spherical Bessel function [$j_n(kr)$], a spherical Hankel function of the first kind [$h^{(1)}_n(kr)$], or a spherical Hankel function of the second kind [$h^{(2)}_n(kr)$]. The $\mathbf{V}$ and $\mathbf{W}$ vector multipoles are complete and orthogonal multipole expansions for transverse fields. They are similar to the vector multipole functions and vector spherical harmonics of Stratton,[49] Rose,[50] Edmonds,[51] Greiner and Maruhn,[52] and Jackson.[53] To be consistent with the Maxwell equations, the conventional electric and magnetic fields ($\mathbf{E}$ and $\mathbf{H}$, respectively) are related to $\mathbf{V}$ and $\mathbf{W}$ as follows:

$$\mathbf{E}(\mathbf{r}) = \sum_{n=0}^{\infty} \sum_{m=-n}^{+n} \left[A_{nm}\mathbf{V}_{nm}(\mathbf{r}) + B_{nm}\mathbf{W}_{nm}(\mathbf{r}) \right], \tag{3}$$

$$\mathbf{H}(\mathbf{r}) = -i\eta \sum_{n=0}^{\infty} \sum_{m=-n}^{+n} \left[B_{nm}\mathbf{V}_{nm}(\mathbf{r}) + A_{nm}\mathbf{W}_{nm}(\mathbf{r}) \right], \tag{4}$$

where η is the index of refraction ($\sqrt{\varepsilon\mu}$) and A_{nm} and B_{nm} are arbitrary coefficients. The η = vector multipole definitions of Greiner and Maruhn specify $A_{nm} = k$, $B_{nm} = ik$, and $\eta = 1$.[52]

Since the electric and magnetic fields were given a time dependence of $e^{-i\omega t}$ for the derivation of

the vector multipoles, the radial functions will be spherical Hankel functions of the second kind

for the incident waves, spherical Bessel functions for the interior waves, and spherical Hankel functions of the first kind for the scattered waves[43]

In the simulations, an EM field is imposed on the cylindrical particle pack and the resultant field interactions within the pack calculated. The imposed field is modeled as a plane wave that is expanded into vector multipole functions with the use of partial-wave expansions:

$$\mathbf{e}_x e^{ikz} = \sum_n i^n \sqrt{\pi (2n+1)} \left[\mathbf{W}_{n,+1} + \mathbf{V}_{n,+1} + \mathbf{W}_{n,-1} - \mathbf{V}_{n,-1} \right], \tag{5}$$

$$\mathbf{e}_y e^{ikz} = (-i) \sum_n i^n \sqrt{\pi (2n+1)} \left[\mathbf{W}_{n,+1} + \mathbf{V}_{n,+1} - \mathbf{W}_{n,-1} + \mathbf{V}_{n,-1} \right]. \tag{6}$$

Note that the partial-wave expansions for the incident plane waves use multipole functions with spherical Bessel functions for the radial dependence rather than spherical Hankel functions of the second kind.

To simulate multiple scattering in a suspension of spherical particles, the iterative multipole approach calculates the Mie scattering solutions for the individual spheres for an arbitrary incident wave field. The scattered wave fields from each sphere are then transformed to the coordinate systems of the other spheres using vector addition theorems for spherical wave functions. The vector addition theorems expand the multipole moments of one sphere in terms of the multipole moments of another sphere, and have the following form:

$$\mathbf{V}'_{\nu\mu} = \sum_{n=0}^{\infty} \sum_{m=-n}^{n} \left(S_{\nu\mu nm} \mathbf{V}_{nm} + T_{nm} \mathbf{W}_{nm} \right), \tag{7}$$

$$\mathbf{W}'_{\nu\mu} = \sum_{n=0}^{\infty} \sum_{m=-n}^{n} \left(S_{\nu\mu nm} \mathbf{W}_{nm} + T_{\nu\mu nm} \mathbf{V}_{nm} \right), \tag{8}$$

where $\mathbf{V}_{nm}$ and $\mathbf{W}_{nm}$ are wave fields scattered from the originating sphere (designated α with coordinates r_α, θ_α, and ϕ_α), and $\mathbf{V}$ and $\mathbf{W}$ are the same wave fields incident on a second sphere (designated β with coordinates r_β, θ_β, and ϕ_β). Since the scattered wave fields

$\mathbf{V}_{nm}$

and $\mathbf{W}_{nm}$ are outgoing, their radial dependence is represented with a Hankel function of the first

kind. However, the incident wave fields $\mathbf{V}_{\nu\mu}$ and $\mathbf{W}_{\nu\mu}$ are represented by a spherical Bessel function in a manner similar to the partial wave expansions. The translation coefficients $S_{\nu\mu}^{nm}$ and $T_{\nu\mu}^{nm}$ are the following:

$$S_{\nu\mu}^{nm} = Z_{\nu,\nu,\mu}^{n,n,m}, \tag{9}$$

$$T_{\nu\mu}^{nm} = i\sqrt{2\nu+1}\,Z_{\nu+1,\nu,\mu}^{n,n,m}, \tag{10}$$

where

$$Z_{\lambda,\nu,\mu}^{l,n,m}(\mathbf{R}_{\alpha\beta}) = \sum_{p=|l-\lambda|}^{l+\lambda} i^{\lambda-l-p} h_p^{(1)}(kR_{\alpha\beta}) Y_{p,m-\mu}(\Theta_{\alpha\beta},\Phi_{\alpha\beta}) \times C_{\lambda,0,p,0}^{l,0}\sqrt{\frac{4\pi(2\lambda+1)(2p+1)}{2l+1}} \sum_{\tau=-1}^{1} C_{l,m-\tau,1,\tau}^{n,m} C_{\lambda,\mu-\tau,1,\tau}^{\nu,\mu} C_{\lambda,\mu-\tau,p,m-\mu}^{l,m-\tau}. \tag{11}$$

Here, $\mathbf{R}_{\alpha\beta} = \mathbf{R}_\alpha - \mathbf{R}_\beta$, and $\mathbf{R}_\beta$ are the position vectors for the two spheres with where $\mathbf{R}_\alpha$ respect to a common origin. The *C* symbols are Clebsch-Gordan coefficients. The vector addition theorems and corresponding translation coefficients can be calculated using recurrence formulas that significantly reduce the number of operations for their computation.[54,55] A more concise form for Eq. (11) is found in Fuller and Mackowski.[56]

The vector addition theorems couple the electromagnetic interactions between all of the spheres in the simulated sphere packing, and therefore form a set of linear equations linking the interactions between all p particles. Since a particular multipole moment from each sphere is

expanded in terms of a sum ofmultipole moments at each of the other spheres, all of the multipole moments will be coupled as well and will require simultaneous solution. This coupling of multipole moments is in contrast to Mie scattering from a single spherical particle,

where all of the multipole moments are decoupled and can be solved independently to obtain the scattered wave field amplitudes. For multiple-scattering from p particles with $n_{\max}$ multipole moments, where $n_{\max}$ is the maximum multipole expansion order computed, there will be $(n_{\max}+1)^2$ moments for each particle coupled to $(n_{\max}+1)^2$ moments for every other particle. The resulting set of linear equations therefore has $p(n_{\max}+1)^2$ equations each with $p(n_{\max}+1)^2$ terms, producing a matrix with $p^2(n_{\max}+1)^4$ elements. Even for modest values of p and $n_{\max}$ (e.g., $p \approx 100$ and $n_{\max} \approx 10$) this set of equations is numerically challenging. This study therefore employed an iteration process to solve the multiple-scattering matrix equations.

Multiple scattering was simulated by updating the incident field on each particle with the scattered wave field contributions from the other particles. The Mie scattering from each particle was then recalculated and translated to the other particles to update the incident fields in an iterative process. This process was repeated until the wave fields converged to a user-specified tolerance. Each iteration step therefore represented an order of scattering, with no iteration (no multiple scattering) representing zero-order or single scattering, the first iteration representing first-order scattering, and so forth. Most of the simulations converged by the second iteration step with a convergence tolerance of 10^{-6} (i.e., a subsequent solution varied from the preceding solution by less than 10^{-6}). Although the iterations are computed sequentially in time, the actual multiple-scattering process itself is time independent. This is equivalent to the direct, simultaneous solution of the entire set of $p(n_{\max}+1)^2$ linear equations. The zero-order scattering, first-order scattering, and so forth therefore represent increasingly accurate degrees of approximation to the multiple scattering solution, and not a time-dependent process.

All of the simulations were computed to a maximum multipole expansion order of $n_{max} = 7$, which has been shown to be necessary for convergence of the solutions by previous convergence studies on random and ordered particle packs.[43] The rapid convergence of the computations can be attributed to the small (200 μm) diameter of the particles as compared to the wavelengths of the 0.01-10.0 GHz EM fields. These values correspond to size parameters of 2×10^{-5} to 2×10^{-2}. The size parameter is defined as $2\pi a/\lambda$, where a is the particle radius and λ is the EM field wavelength. Although the size parameters are within the Rayleigh scattering approximation for single spheres and therefore suggest only small values (< 7) are required for n_{max}, previous studies have demonstrated that higher n_{max} values are necessary when multiple scattering is involved.[43] Computer algorithms for the model were written and compiled in FORTRAN 90 with double precision. Simulations were performed on a personal desktop computer with 2.0 gigabytes random access memory and a 3.2-GHz processor.

The effective permittivity was calculated by averaging the $\mathbf{E}$ and $\mathbf{D}$ fields over a representative volume containing the particles and matrix, and then taking the ratio of the volume-averaged fields:

$$\varepsilon_{eff} = \frac{\langle \mathbf{D} \rangle}{\langle \mathbf{E} \rangle} . \qquad (12)$$

The averaging was performed by evaluating the $\mathbf{E}$ and $\mathbf{D}$ fields on a uniformly spaced three-dimensional grid containing $37^3 = 50{,}653$ points. For non-aggregated particle suspensions the evaluation grid comprised a cube containing approximately 70 particles (0.10 vol. fraction) to 420 particles (0.60 vol. fraction). Since the electric field was polarized in the x direction in the simulations, only the x components of the electric field and electric displacement were used to compute the effective permittivity. This was equivalent to the use of a parallel-plate capacitor

for measuring the dielectric constant, and provided results physically comparable to experimental methods.[43]

The volume of the cubic evaluation grid comprised 2.5% of the volume of the cylindrical packing of spheres (cube edge length = 0.27 pack diameter). The simulation results were not independent of the cube volume or position. Decreasing the cube volume increased the variability of the results since local fields within and around the particles were sampled to an increasing extent. These local field effects were particularly strong for aggregated particle packs. Increasing the cube volume increased edge effects due to the boundary of the particle pack which introduced greater error into the computations. Similarly, placing the cube near the sides of the particle pack also increased edge effects. The volume and position of the evaluation grid was therefore optimized in a previous study to minimize variation and maximize accuracy by comparing simulations of ordered particle packings to exact lattice models.[43] The cube volume was determined to simultaneously minimize local field effects and edge effects, whereas the cube was positioned at the center of the particle pack to minimize edge effects and maximize the electric field uniformity.

B. Effective medium models

As a comparison for the simulation results, macroscopic permittivities for aggregate microstructures were also calculated using effective-medium models. The effective-medium models were constructed from successive application of effective-medium formulas originally derived for microstructures with uniformly distributed particles [Fig. 1(a)]. For cluster aggregation, the particle clusters were modeled as single, large quasi-particles comprised of the smaller particles [Fig. 1(b)]. An effective permittivity was first calculated for the interior of the

quasi-particle by treating it as a medium with uniformly distributed particles. Since the particles within the quasi-particle had a higher volume fraction than the average volume fraction for the material due to their aggregation, the permittivity for the quasi-particle was different than that for the medium as a whole. The macroscopic permittivity for the medium was then obtained by applying the effective-medium formula to the quasi-particles in the air matrix. In this case, the quasi-particles were modeled as solid particles with the quasi-permittivity as calculated in the first step and with a quasi-volume fraction (volume fraction of clusters in medium).

A similar approach was used to model the aggregation of particles to form large spherical voids (foaming). In this case, a quasi-matrix was modeled as a medium uniformly filled with the particles [Fig. 1(c)]. The effective-medium formula was first applied to the interior of the quasi-matrix to obtain its effective permittivity. Again, the particles within the quasi-matrix displayed a higher volume fraction than the average volume fraction for the material, yielding a permittivity different from that of the medium as a whole. Finally, the quasi-matrix was modeled as a solid matrix with a quasi-permittivity, a quasi-volume fraction, and large spherical voids to obtain the macroscopic permittivity of the medium.

The first effective-medium model was generated from the Maxwell Garnett equation:[25]

$$\varepsilon_{eff} = \varepsilon_0 + 3f\left(\frac{\varepsilon_1 - \varepsilon_0}{\varepsilon_1 + 2\varepsilon_0 - f(\varepsilon_1 - \varepsilon_0)}\right). \quad (13)$$

The inclusion (particle or void), matrix, and effective permittivities are ε_1, ε_0, and ε_{eff}, respectively. The inclusion volume fraction is f. Equation (13) has been characterized as a first-order approximation accounting for dipole-dipole interactions between particles in the suspension, and is extensively used to this day for many scattering and effective medium calculations across many fields of application.[29] However, multipole computations of up to 3600

particles have shown that the Maxwell Garnett equation provides results most consistent with a single-scattering model having no particle-particle interactions.[43] Equation (13) can therefore be regarded as only a zero-order approximation.

The second effective-medium model was generated from an equation derived by Torquato.[26] This equation originates from a microstructure-dependent model based on a perturbation expansion of the polarization that yields a set of microstructure-dependent parameters known as point probability functions. Truncation of the expansion provides the following approximate formula for three-dimensional microstructures:

$$\frac{\varepsilon_{eff}}{\varepsilon_0} = \left\{ \frac{1 + 2f\delta - 2(1-f)\zeta\delta}{1 - f\delta - 2(1-f)\zeta\delta^2} \right\}. \quad (14)$$

The microstructure-dependent three-point parameter ζ is a function of f. The parameter δ is

$$\delta = \frac{\varepsilon_1 - \varepsilon_0}{\varepsilon_1 + 2\varepsilon_0}. \quad (15)$$

Torquato provides three-point parameter values for f = 0.10-0.60 for random microstructures of impenetrable spheres.[26] Note that the Maxwell-Garnett equation was originally formulated to calculate the effective properties (conductivity, permittivity, etc.) of media containing uniformly distributed inclusions [Fig. 1(a)], whereas the Torquato equation is capable of modeling higher-order microstructures [Figs. 1(b) and 1(c)] for properly calculated ζ parameters. For this study, the ζ parameters for uniformly random particle packs as calculated in Ref. 26 were used to construct the effective medium model. Although ζ parameters and corresponding Torquato

models can be directly constructed for aggregated microstructures, this initial study did not

address these models.

III. RESULTS

The effects of the level of particle aggregation on effective permittivity were determined by keeping the average particle volume fraction constant in the medium and modeling the permittivity as a function of local particle volume fraction in the cluster or foam wall. For example, Fig. 2 displays simulated foam-type microstructures of 1,212 particles. The microstructure initially had a uniform distribution and average volume fraction of 0.30 [Fig. 2(a)]. The level of particle aggregation was increased in subsequent microstructures by increasing the void size and the corresponding local particle volume fraction to 40% [Fig. 2(b)], 50% [Fig. 2(c)], and 60% [Fig. 2(d)]. Average particle volume fractions of 0.20 and 0.30 were used for this study, similar to highly dual porous media,[12] with the local particle volume fractions having a maximum of 0.50 and 0.60, respectively. For comparison, the volume fraction for a maximally random jammed packing of hard monodisperse spheres is ~0.64-0.65.[57]

Figure 3 displays grayscale plots of the 10-MHz microscopic electric field amplitudes for the foam-type microstructures shown in Fig. 2. The plots reveal low field strengths within the particles, intermediate field strengths in the large void regions, and high field strengths between closely spaced particles. The plots also reveal that the range of electric field amplitudes increases with increasing aggregation. Table 1 shows the range of electric field amplitudes as a function of local particle-volume fraction, with increasing volume fraction proportional to degree of aggregation (no aggregation for 0.30; maximum aggregation for 0.60). The results indicate that aggregation increases microscopic field amplitudes, probably due to the increased localized packing of particles.

Figure 4 shows the effective permittivities at 10 MHz for cluster-type and foam-type microstructures constructed from a Monte Carlo algorithm[45] and with an average particle

volume fraction of 0.30. All three models predicted that foaming of the microstructure increases the effective permittivity for $\varepsilon_1 > \varepsilon_0$. The model results disagreed, however, for cluster aggregation. While the Maxwell Garnett model showed no change in permittivity due to clustering, the Torquato model showed an increase in permittivity with local particle volume fraction. In contrast, the multipole model showed a 3.1 ± 1.4% decrease in effective permittivity for clustering with a highly significant probability (R = -0.75 for 15 simulations). R is the coefficient of linear correlation defined by the covariance divided by the standard deviations:

$$R = \frac{\sigma_{xy}}{\sigma_x \sigma_y} = \frac{\sum (x_i - \bar{x})(y_i - \bar{y})}{\sqrt{\sum (x_i - \bar{x})^2 \sum (y_i - \bar{y})^2}}. \qquad (16)$$

The multipole model also displayed a 3.0 ± 1.6% increase for foaming, but with only a significant correlation (R = 0.53; 20 simulations).

To verify the 0.30 volume fraction results for the multipole model, cluster and foam simulations were also performed for a constant average volume fraction of 0.20 and using particle packs constructed from a different algorithm (reduced dimension).[46,47] The results, Fig. 5, show the same trends as in Fig. 4, but with much smaller standard deviations in the 10-MHz permittivity values. For cluster-type aggregation the effective permittivity decreased by 3.2 ± 0.2%, whereas for foam-type aggregation the effective permittivity increased by 1.3 ± 0.4% (note that the foam simulations only went to 0.4 local particle volume fraction as compared to 0.5 for the cluster simulations). The smaller deviations can be attributed to a larger number of particles used in the 0.20 simulations (~ 2400) than for the 0.30 simulations (~ 1200). The smaller deviations yield much higher correlation results for both aggregation (R = -0.98; 15 simulations) and foaming (R = 0.90; 15 simulations). The results for the Maxwell Garnett model at 0.20

volume fraction are also shown for comparison.

Figure 6 shows the effects of aggregation on effective permittivity for a medium where the dielectric constants have been reversed between the particles and matrix ($\varepsilon_1 = 1.0$ $\varepsilon_0 = 8.5$, and respectively). This "reverse-constant" medium is essentially that of spherical voids in a solid matrix, and the behavior of the effective permittivity is reversed as well when compared to the behavior of a "normal" medium (solid particles in air or vacuum). Clustering of the voids increased the permittivity by 2.2 ± 0.07% with a highly significant correlation (R = 0.98; 15 simulations). Foaming of the voids decreased the permittivity by 0.84 ± 0.33% with a significant correlation (R = -0.85; 15 simulations). The Maxwell Garnett model for the reverse-constant medium agrees well with the multipole simulations for foaming, but strongly disagrees with the simulations for clustering.

The results from both the effective medium models and the multipole model were consistent in showing increases in the effective permittivity of particle aggregates with foam-type microstructures. The results between the models were not consistent, however, for particle aggregates with cluster-type microstructures. Since the multipole model directly computes the effective permittivity from multiple-scattering interactions in the particle pack, its results are expected to be more reliable than those from the effective-medium approximations that use the Maxwell Garnett and Torquato formulas that only provide an estimate of the multiple-scattering effects. The high degree of statistical significance and correlation for the multipole simulation results in Figs. 4-6 supports this conclusion.

In addition to the 10-MHz (0.01-GHz) simulations, simulations were also performed on the 0.20-volume fraction particle packs at 0.1, 1.0, and 10.0 GHz to determine the effect of frequency on the aggregation-induced permittivity values. The results, Fig. 7, show very little

change in the effective permittivity values as a function of frequency. The only significant

change is a slight decrease between 1.0 and 10.0 GHz. However, this decrease represents only a 1% drop in permittivity, and is independent of the degree of aggregation. Since the scattering interactions are dependent on the product of the EM field wave vector and scatterer size [*kr* in Eqs. (1) and (2)], an increase or decrease in the wavelength of the incident wave can be viewed as a decrease or increase in the scale of the scattering heterogeneities of a medium, respectively. Since the frequency is inversely proportional to the wavelength of the EM wave field, Fig. 7 therefore indicates a significant degree of scale invariance of the permittivity as a function of the size of the aggregate (heterogeneity) length scale.

IV. DISCUSSION

A. Comparison of results

Deviations between the results for the Maxwell Garnett, Torquato, and iterative multipole models were expected since previous studies with ordered and random microstructures had shown large deviations as well.[43] In the previous studies, the model predictions were compared to those from (1) exact lattice models that used symmetry and periodicity to provide exact solutions for the permittivities and (2) experimental measurements of random glass sphere packings in air. The results showed that the multipole simulations and Torquato model were in greater agreement with the exact lattice models and experimental measurements than the Maxwell Garnett model. The Maxwell Garnett model was more in agreement with single-scattering results (no multiple scattering), and was therefore concluded to be only a zero-order approximation since it did not account for particle-particle interactions or microstructure.

The results for the reverse-constant medium (voids in a solid matrix) are physically consistent with those for a normal medium (solid particles in air or vacuum). As the voids

aggregate, they form void clusters that are analogous to the large voids of a normal foam microstructure with solid particles. Both clustering in the reverse-constant medium (Fig. 6) and foaming in the normal medium (Fig. 5) therefore display an increase in the effective permittivity. Similarly, foaming in the reverse-constant medium creates large, spherical regions of solid matrix material that are analogous to the clusters of solid particle in a normal medium. Therefore, both foaming in the reverse-constant medium (Fig. 5) and clustering in the normal medium (Fig. 6) exhibit a decrease in the effective permittivity.

In this study, the disagreement between the Torquato and multipole results can be attributed to the assumption used in the two-level effective-medium model developed from the Torquato equation. This assumption was that the local permittivity of the quasi-particle or quasi-matrix could be calculated using the local particle volume fraction within the quasi-particle or matrix and assuming it was a separate, infinite medium. However, local geometric effects due to the finite sizes of the quasi-particles or voids within the quasi-matrix would be neglected with this approximation. In contrast, the multipole method directly calculated the field interactions from all of the particle locations in the medium, thus providing a more accurate simulation of aggregation effects. No effective-medium assumptions were used in the multipole method, so the effects of the aggregation geometry (cluster and void sizes) were modeled more accurately. Validation of the multipole results with experimental data will be required, however, to test the accuracy of the model and more fully understand the effects of aggregation on effective permittivity in particulate media. Given the sensitivity of current measurement methods, this remains a considerable challenge.

B. Multiscale or hierarchical porosity structures

Aggregation of monodisperse spheres creates microstructures with multiscale or hierarchical porosity structures. In this study, dual-porosity structures were produced for cluster and foam aggregation. The large-scale level of porosity consisted of the regions between the particle clusters or within the large spherical voids of the particle foam. The small-scale level of porosity consisted of the interparticle regions within the clusters or foam walls. The results of the numerical model indicate that these multiscale or hierarchical microstructures affect the effective permittivity of heterogeneous materials. This conclusion is relevant for measurements of media that may undergo microstructural alterations such as soils (aggregation of soil grains), fluids in sedimentary rocks (differential wetting at different porosity scales), composites (particle aggregation during manufacture), biological tissues (tissue remodeling due to neoplasms and other pathologies), and fluid suspensions (flocculation, etc.).

Cluster-type aggregation forms large quasi-particles with small-scale porosity within the quasi-particle. This type of microstructure is comparable to a dual-porosity microstructure comprised of random, uniformly distributed solid particles with small, internal, spherical voids. Because of this similarity, we would expect the effective permittivity of the particles with internal voids to be similar to that of cluster aggregation and therefore lower than that of a simple random microstructure for an equal solid volume fraction [Fig. 1(a)]. To test this hypothesis, the numerical model was applied to a random microstructure of particles containing internal voids. Using the multipole simulations, an effective permittivity for the particles was first calculated for spherical voids within the solid particle phase. This permittivity was then used for the particles to calculate the effective permittivity of the total particle pack. The computational results showed a 1.4% decrease in overall effective permittivity with an increase in internal porosity of 0

to 0.60 volume fraction pores (constant 0.30 solid volume fraction). The numerical results disagreed with those from an effective-medium model based on the Maxwell Garnett equation, however, which showed an increase in effective permittivity of 11% for the same increase in pore volume fraction.

C. Proposed mechanisms

Three theories are proposed to explain the changes in permittivity with aggregation in this study. The first theory involves a waveguide-like mechanism where the wave fields are concentrated to a greater degree in specific regions of the heterogeneous structures. The speed of EM wave propagation in a medium is inversely proportional to the square root of its permittivity. On a microscopic scale, spatial variations in the local permittivity of a complex medium will lead to spatial variations in the wave propagation behavior and produce phenomena such as wave guiding, wave trapping, and photonic band gaps. These propagation anomalies will give rise to changes in the effective permittivity. Similarly, the microscopic propagation behavior of EM fields in an aggregated material will be a function of the level and type of particle aggregation, and will influence the material's effective permittivity.

Aggregation in random particle suspensions produces a quasi-continuous phase (e.g., the quasi-matrix in Fig. 1) of higher or lower particle density, thus higher or lower permittivity, in the medium. The simulations indicate that the effective permittivity changes in aggregated microstructures follow the same trends as the local permittivity changes in the quasi-continuous phase. The quasi-continuous phase thus appears to function as a preferred path for wave field propagation due to its continuity through the microstructure. The resultant macroscopic wave

field propagation and effective permittivity therefore reflects the wave guiding influence and local permittivity of the aggregation paths in the suspension.

For foam-type microstructures, the particles condense to form continuous paths where the particle volume fractions are greater than in the rest of the suspension. These paths therefore have wave field velocities less than the uniform random structure due to the higher permittivities of the particles, and also function as waveguides for wave field propagation through the particle suspension due to their continuity or connectivity. Since the wave field velocities are less in the paths than in the non-aggregated microstructure, the effective permittivity for foam-type aggregation increases.

Similarly for cluster-type microstructures, the interstitial voids condense to form continuous paths where the particle volume fractions are less than in the rest of the suspension. These paths therefore have wave field velocities greater than the uniform random structure due to the lower permittivity of the matrix (air or vacuum). Again, the paths function as waveguides for wave field propagation through the particle suspension due to their continuity or connectivity. Since the wave field velocities are greater in the paths than in the non-aggregated microstructure, the effective permittivity for cluster-type aggregation decreases.

A second theory attributes the simulation results to a percolation-like mechanism. This mechanism is also consistent with the simulation results for the aggregated suspensions, and is analogous to electrical conduction in amorphous and granular systems resulting from tunneling percolation. In this theory, higher permittivities are expected for foam microstructures because of the continuous paths of the closely spaced particles of high-permittivity (similar to a path of stepping stones), whereas lower permittivities are predicted for cluster microstructures because the clusters isolate the high-permittivity particles and do not provide continuous paths. The

difference between the proposed mechanism and percolation in conductive systems is the absence of a percolation threshold. This is because wave field propagation through a random particle suspension relies on the local particle density (volume fraction), which is continuous, and not on particle-to-particle contacts, which are discrete. Although percolation theory was developed to model electrical conduction in conductor-insulator systems, it has been extended to other macroscopic properties including elasticity and viscous fluid flow.[58] The application of percolation-like processes to the dielectric properties of complex media may therefore provide new insights into the physics of these systems, and may offer new models for other physical systems such as amorphous materials or elastic wave fields in heterogeneous materials.

Tunneling percolation is a particularly interesting analog for modeling the dielectric permittivity of aggregated microstructures. In this approach, virtual charges are envisioned as tunneling from one particle to the next to emulate the multipole interactions and polarization effects in heterogeneous materials. Like the probability of conduction tunneling in a particulate system, multipole fields also decrease with distance from the particle. However, whereas conduction tunneling drops off exponentially, multipole fields exhibit a power-law drop.[59-62] Also, instead of electrons tunneling from one inclusion to the next as in standard percolation models, in the dielectric case polarization charges would appear to tunnel from one inclusion to the next. Therefore, polarization effects would propagate more strongly in microstructures with closely spaced particles in quasi-continuous paths as in Fig. 1(c), and the effective permittivity would be higher. Conversely, the intercluster distances between the particles in cluster-type aggregation, Fig. 1(b), would limit the tunneling of polarization charges and thus suppress the multipole interactions. The permittivity would therefore be more representative of the background matrix between the clusters.

A third mechanism for the simulation results is that the second-order microstructures in the aggregated suspensions—the particle clusters or large voids—give rise to collective polarization effects that enhance or diminish the background polarization field arising from the first-order microstructure (uniformly random suspension). These polarization effects would be similar to the asymmetry predicted by the Maxwell Garnett equation [Eq. (13)], where voids in a solid matrix produce higher effective permittivities than solid particles in an air/vacuum matrix for the same solid volume fraction. For the aggregated structures, collective polarization effects would cause the particle clusters to behave as quasi-particles and the large voids to behave as quasi-voids (Fig. 1). Collective polarization effects may also be responsible for the waveguide-like behavior, where enhanced polarization on the boundaries between the second-order microstructures (quasi-particles and quasi-matrix) would concentrate the EM field in the quasi-matrix.

Interestingly, the changes in permittivity with aggregation observed in this study mirror those of ordered arrays of particles. Exact theory and multipole simulations both show that simple-cubic (sc) lattices and random packings have higher permittivities than body-centered-cubic (bcc), face-centered-cubic (fcc), and hexagonal-close-packed (hcp) lattices for packings of equal volume fraction.[43] Since sc lattices and maximally random packings have a lower coordination number (6) than bcc (8), fcc (12), and hcp (12) lattices, the particles in these structures will be 11% (compared to fcc and hcp) to 17% (compared to bcc) closer to their nearest neighbors for equal volume-fraction packings. This creates a more open, foam-like structure for the sc and random structures, with larger interstices and void spaces than the bcc, fcc, or hcp lattices. Additionally, the closer particles create more defined pathways for a waveguide or percolation-like mechanism. The permittivities for the sc and random structures are therefore

correspondingly higher. The greatest difference in permittivity is between the sc and bcc lattices, which also show the greatest difference in nearest neighbor distances (17%). More open lattice structures are also possible such as the diamond lattice for particles with a coordination number of 4. Note that several solid electrolytes such as cubic ZrO_2 have a fluorite crystal structure, a derivative of the diamond structure. These crystals have an open, foam-like structure that provides channels for the diffusion of oxygen.

D. Applicability of the quasistatic limit

The simulation results showed that subtle changes in microstructure produced statistically significant changes in the effective permittivity for random suspensions of spheres, even though the particle diameters and corresponding aggregation structures were 2-5 orders of magnitude smaller than the incident field wavelength in free space (30 m for 10-MHz waves to 3 cm for 10-GHz waves). This conclusion runs counter to a commonly accepted interpretation of the quasistatic limit. This interpretation holds that a composite can be considered homogeneous if the length scales of the heterogeneities are much smaller than the wavelength of EM field.[31] This interpretation is equivalent to the Rayleigh assumption of uniform field strength. The quasistatic limit has also been used to argue that EM scattering will not be significant in heterogeneous media at long wavelengths, and thus the EM field will be insensitive to microstructural variations at the size scale of the inclusions.[36,37] However, the aggregation results in this study showed that small changes in microstructure affected macroscopic properties in the quasistatic limit, although the macroscopic composition (average particle volume fraction) remained constant. Additionally, the simulation results were by and large insensitive to the scale of the heterogeneities with respect to the incident field wavelength.

The results of this study show that the uniform field strength assumption may not be valid for the dielectric properties of many ordinary microstructures, and its use should be carefully scrutinized for future research in this area. The effects of subtle microstructural changes such as aggregation also indicate the importance of accounting for all of the collective interparticle interactions (scattering) with a level of detail beyond that of conventional effective medium theories [Eqs. (13) and (14)]. Multipole simulations of soot particle clusters in the electrostatic limit have also shown that particle-particle interactions with multipole orders higher than the Rayleigh-limit dipole are necessary to accurately predict the optical absorption properties of the clusters.[63]

E. Applications

Interest in wave propagation in heterogeneous media has grown over the past decades due to the development of remote and *in situ* sensing methods for geophysics, medical physics, nondestructive evaluation, space exploration, and other fields of science and technology. Relating effective properties such as the permittivity to the material microstructure is crucial to evaluating sensor data and extracting information about the interrogated medium. Additionally, the development of new composites with novel or enhanced properties has spurred efforts to predict the properties of heterogeneous media and engineer their microstructures to optimize these new effects.[14]

The iterative multipole approach used in this study is a very efficient and direct method for simulating the multiple-scattering interactions of EM fields in suspensions of spherical particles. The modeling permits analysis of material response that is difficult or impossible with current experimental methods. The approach is amenable to the simulation of particles with

polydisperse sizes and properties, and in arbitrary microstructures including ordered, random, and hierarchical configurations.[43,64,65] Simulations of materials with structured (layered or with internal inclusions) and nonspherical (spheroidal) particles are also feasible with the iterative multipole approach.[56,64-66] The iterative multipole approach may therefore provide a crucial link between microscopic structure and macroscopic properties for model-based signal analysis tools.

Although the changes in effective permittivity calculated by the simulation models appear small and bounded by ±3%, the ability to predict these variations in material properties due to microstructure may be helpful in establishing expected variances in measurements, in determining the accuracy of data interpretations, and in predicting material property variations in composites. The largest permittivity differences are approximately 6% observed between maximally aggregated foam and cluster microstructures. Although not large when compared with other factors that impact remote sensing or composite properties, it is expected that this effect will become more pronounced in suspensions with non-spherical particles. The simulations in this work therefore provide the fundamental groundwork for further study on more complex geometries, especially in the frequency domain, and may lead to new applications of microwave measurement methods to determine material properties. Additionally, understanding this source of variation in the data will contribute to our understanding of the sources of noise in remote sensing and geophysical data, as well as material property variability in composites Finally, if complementary measurements are available that can provide information on a material's composition, density, and particle size distribution, multipole simulations may be able to provide sufficient accuracy to predict the material's microstructure with a high degree of confidence.

V. CONCLUSIONS

Analytical methods for approximating the material properties of particle-filled media, such as the dielectric properties of soil, assume a uniform, random particle distribution. To determine what effect microstructure, and specifically aggregation, has on the effective physical properties of a particle pack, a multipole computer model was used to simulate wave propagation and scattering in simulated non-uniform packings of monodisperse spheres. Two types of aggregation were examined, aggregates with a cluster-type microstructure and aggregates with a foam-type microstructure. The test packs contained approximately equal numbers of particles with varying degrees of aggregation. It was found that the foam-type microstructures had consistently higher dielectric properties than uniform packings, while the cluster-type microstructures had properties that were consistently lower. The effective permittivity changed by +3.0% (foam-type aggregation) and –3.1% (cluster-type aggregation) at maximum aggregation (local particle volume fraction of 0.60 in aggregated regions). The simulations additionally showed that the ranges for the microscopic electric field values in the particle packs increased with greater aggregation.

Two-stage effective-medium models were also developed for comparison to the multipole model results. The effective-medium models displayed trends for foams that were consistent with the multipole models, showing an increasing effective permittivity. They were not consistent for clusters, however, showing increasing or constant effective permittivities whereas the multipole models displayed decreasing trends. The disagreement between the models is due in part to the assumption in the first stage of the effective-medium models that calculates the permittivity of the aggregated region (cluster or foam matrix) by assuming it is an infinite medium with the local particle volume fraction.

The effective permittivity changes in aggregated microstructures can be attributed to one of three processes. The first process is a waveguide-like mechanism of preferred wave field propagation through the quasi-continuous phase that forms paths of higher or lower particle density, thus higher or lower permittivity, through the medium. The increase or decrease in effective permittivity therefore parallels the increase or decrease in local permittivity of the continuous matrix network, but is opposite to the local permittivity changes in the particle clusters (cluster-type aggregation) or large voids (foam-type aggregation). The second process is a percolation-type mechanism that views the multipole interactions as a type of tunneling phenomenon where polarization charges tunnel, in a virtual sense, from one particle to another in the presence of an external electric field. This process links the particle-to-particle multipole interactions to the multiscale heterogeneity of the microstructure. The percolation-like process is similar to tunneling percolation in conductor-insulator systems, but lacks a critical threshold since it is a function of particle volume fraction, which is continuous. The third mechanism ascribes the permittivity results to collective polarization effects arising from the particle clusters or large voids. These secondary polarization fields would modify the primary polarization field caused by the underlying random particle distribution.

The simulation results displayed no change with frequency from 0.01 to 1.00 GHz, and only a 1% drop in effective permittivity values for 10.0 GHz. The results also showed that EM fields with wavelengths 2-5 orders of magnitude greater than the scale of the microstructural features can detect subtle microstructural changes that do not alter the overall density, composition, or random disorder of the material. The quasistatic limit has to therefore be carefully interpreted for the simulated microstructures and conditions.

ACKNOWLEDGMENTS

The authors thank Brent L. Carruth for his work on the iterative multipole approach and I. Lee Davis for supplying the random particle microstructures generated by the reduced-dimension algorithm for the 0.20-volume fraction studies.

REFERENCES

[1] M. Faraday, *Experimental Researches in Chemistry and Physics* (Taylor and Francis, London, 1991).

[2] J. C. Maxwell, *A Treatise on Electricity and Magnetism* (Clarendon, London, 1873), Vol. 1.

[3] R. S. Rayleigh, Philos. Mag. **34**, 481 (1892).

[4] S. Torquato, *Random Heterogeneous Materials: Microstructure and Macroscopic Properties* (Springer-Verlag, New York, 2002).

[5] R. Zallen, *The Physics of Amorphous Solids* (Wiley, New York, 1983).

[6] R. Knight and A. L. Endres, in *Near Surface Geophysics (Investigations in Geophysics, No. 13),* edited by D. K. Butler (Society of Exploration Geophysicists, Tulsa, 2005).

[7] D. A. Robinson, S. B. Jones, J. A. Wraith, D. Or, and S. P. Friedman, Vadose Zone J. **2**, 444 (2003).

[8] T. J., Schmugge, W. P. Kustas, J. C. Ritchie, T. J. Jackson and A. Rango, Adv. Water Res. **25**, 1367 (2002).

[9] R. Knight, Annu. Rev. Earth Planet. Sci. **29**, 229 (2001).

[10] S. B. Jones and S. P. Friedman, Water Resour. Res. **36**, 2821 (2000).

[11] S. P. Friedman and D. A. Robinson, Water Resour. Res. **38**, 1236 (2002).

[12] J. M. Blonquist, Jr., S. B. Jones, I. Lebron, and D. A. Robinson, Water Resour. Res. **42**, W05424 (2006).

[13] T. Miyamoto, T. Annaka, and J. Chikushi, Vadose Zone J. **2**, 90 (2003).

[14] C. Brosseau and A. Beroual, Prog. Mater. Sci. **48**, 373 (2003).

[15] M. R. Haberman and Y. H. Berthelot, J. Appl. Phys. **102**, 124903 (2007).

[16] L. Jylhä, J. Honkamo, H. Jantunen, and A. Sihvola, J. Appl. Phys. **97**, 104104 (2005).

[17] K. R. Lauer in *Handbook on Nondestructive Testing of Concrete*, edited by V. M. Malhotra and N. J. Carino (CRC, Boca Raton, 1991).

[18] P. M. Roberts in *Nondestructive Testing Techniques*, edited by D. E. Bray and D. McBride (Wiley, New York, 1992).

[19] E. Prodan, C. Prodan, and J. H. Miller, Jr., Biophys. J. **95**, 4174 (2008).

[20] K. Asami, E. Gheorghiu, and T. Yonezawa, Biophys. J. **76**, 3345 (1999).

[21] G. Emili, A. Schiavoni, M. Francavilla, L. Roselli, and R. Sorrentino, IEEE Trans. Microwave Theory Tech. **51**, 178 (2003).

[22] R. Goodman and M. Blank, J. Cell. Physiol. **192**, 16-22 (2002).

[23] X. Li, E. J. Bond, B. D. Van Veen, and S. C. Hagness, IEEE Antennas Propag. Mag. **47**, 19 (2005).

[24] M. Lazebnik, M. C. Converse, J. H. Booske, and S. C. Hagness, Phys. Med. Biol. **51**, 1941 (2006).

[25] J. C. Maxwell Garnett, Phil. Trans. R. Soc. London, Ser. A **203**, 385 (1904).

[26] S. Torquato, J. Appl. Phys. **58**, 3790 (1985).

[27] P. N. Sen, C. Scala, and M. H. Cohen, Geophysics **46**, 781 (1981).

[28] A. Sihvola and J. A. Kong, IEEE Trans. Geosci. Remote Sens. **26**, 420 (1988).

[29] A. Sihvola, *Electromagnetic Mixing Formulas and Applications* (The Institution of Electrical Engineers, London, 1999).

[30] C. Brosseau, J. Phys. D.: Appl. Phys. **39**, 1277 (2006).

[31] A. Mejdoubi and C. Brosseau, J. Appl. Phys. **102**, 094105 (2007).

[32] I. Krakovsky and V. Myroshnychenko, J. Appl. Phys. **92** (11), 6743 (2002).

[33] E. Tuncer, S. M. Gubański, and B. Nettelblad, J. Appl. Phys. **89** (12), 8092 (2001).

[34] V. Myroshnychenko and C. Brosseau, J. Appl. Phys. **97**, 044101 (2005).

[35] V. Myroshnychenko and C. Brosseau, Phys. Rev. E **71**, 016701 (2005).

[36] O. Pekonen, K. Kärkkäinen, A. Sihvola, and K. Nikoskinen, J. Electromagn. Waves Appl. **13**, 67 (1999).

[37] K. K. Kärkkäinen, A. H. Sihvola, and K. I. Nikoskinen, IEEE Trans. Geosci. Remote Sensing **38**, 1303 (2000).

[38] C. Blanchard, J. A. Porti, J. A. Morente, A. Salinas, and E. A. Navarro, J. Appl. Phys. **102**, 064101 (2007).

[39] M. Wang and N. Pan, J. Appl. Phys. **101**, 114102 (2007).

[40] P. A. Martin, *Multiple Scattering: Interaction of Time-Harmonic Waves with N Obstacles* (Cambridge, Cambridge, UK, 2006).

[41] P. R. Siqueira and K. Sarabandi, IEEE Trans. Antennas Propag. **48**, 317 (2000).

[42] K. Hinsen and B. U. Felderhof, Phys. Rev. B **46**, 12955 (1992).

[43] T. E. Doyle, D. A. Robinson, S. B. Jones, K. H. Warnick, and B. L. Carruth, Phys. Rev. B **76**, 054203 (2007).

[44] I. Lebron, D. A. Robinson, S. Goldberg, and S. M. Lesch, Soil Sci. Soc. Am. J. **68**, 1549 (2004).

[45] J. L. Finney, Proc. R. Soc. London, Ser. A **319**, 479 (1970).

[46] I. L. Davis and R. G. Carter, J. Appl. Phys. **67**, 1022 (1990).

[47] M. D. Webb and I. L. Davis, Powder Technol. **167**, 10 (2006).

[48] T. E. Doyle, J. Acoust. Soc. Am. **119**, 2599 (2006).

[49] J. A. Stratton, *Electromagnetic Theory* (McGraw-Hill, New York, 1941), Chap. 7.

[50] M. E. Rose, *Elementary Theory of Angular Momentum* (John Wiley and Sons, New York, 1957).

[51] A. R. Edmonds, *Angular Momentum in Quantum Mechanics* (Princeton University Press, Princeton, 1957).

[52] W. Greiner and J. A. Maruhn, *Nuclear Models* (Springer-Verlag, Berlin, 1996).

[53] J. D. Jackson, *Classical Electrodynamics*, 2nd edition (John Wiley and Sons, New York, 1975).

[54] W. C. Chew and Y. M. Wang, J. Electromagn. Waves Appl. **7**, 651 (1993).

[55] D. W. Mackowski, J. Opt. Soc. Am. A **11**, 2851 (1994).

[56] K. A. Fuller and D. W. Mackowski, in *Light Scattering by Nonspherical Particles*, edited by M. I. Mishchenko (Academic Press, San Diego, 2000), Chap. 8.

[57] A. Donev, S. Torquato, and F. H. Stillinger, Phys. Rev. E **71**, 011105 (2005).

[58] S. Feng, B. I. Halperin, and P. N. Sen, Phys. Rev. B **35**, 197 (1987).

[59] I. Balberg, Phys. Rev. Lett. **59**, 1305 (1987).

[60] S. Vionnet-Menot, C. Grimaldi, T. Maeder, S. Strässler, and P. Ryser, Phys. Rev. B **71**, 064201 (2005).

[61] C. Grimaldi and I. Balberg, Phys. Rev. Lett. **96**, 066602 (2006).

[62] N. Johner, C. Grimaldi, I. Balberg, and P. Ryser, Phys. Rev. B **77**, 174204 (2008).

[63] D. W. Mackowski, Appl. Opt. **34**, 3535 (1995).

[64] T. E. Doyle, K. H. Warnick, and B. L Carruth, J. Acoust. Soc. Am. **122**, EL210 (2007).

[65] T. E. Doyle, A. T. Tew, K. H. Warnick, and B. L Carruth, J. Acoust. Soc. Am. **125**, 1751 (2009).

[66] I. R. Ciric and F. R. Cooray, in *Light Scattering by Nonspherical Particles*, edited by M. I. Mishchenko (Academic Press, San Diego, 2000), Chap. 4.

Tables

TABLE I. Range of 10-MHz electric field amplitudes for the foam-type microstructures shown in Fig. 3. The background or imposed electric field amplitude (incident wave) was 1.000. Negative amplitude values indicate a reversal in the direction of the electric field.

Local particle volume fraction	Range		
	Low Value	High Value	Total Range
0.30	0.147	2.513	2.366
0.40	-0.059	2.572	2.631
0.50	-0.114	3.004	3.118
0.60	-0.246	3.453	3.699

Figure Captions

FIG. 1. (a) Random suspension with uniformly distributed spherical particles. (b) Random suspension with particles aggregated into spherical clusters. The clusters are modeled with an effective-medium approach as quasi-particles, where the permittivity of the quasi-particle is first calculated, and then the permittivity of the quasi-particle suspension is calculated. (c) Random suspension with particles aggregated to form spherical voids as in a foam-type microstructure. The foam wall is modeled with an effective-medium approach as a quasi-matrix, where the permittivity of the quasi-matrix is first calculated, and then the permittivity of the void/quasi-matrix suspension is calculated.

FIG 2. Two-dimensional slices through three-dimensional microstructures used for the iterative multipole simulations. Each frame represents a successive aggregation of particles into a foam-like microstructure, with an initial uniform particle volume fraction of 30% (a) evolving to a local particle volume fraction of 40% (b), 50% (c), and 60% (d).

FIG. 3. Grayscale plots of 10-MHz electric field amplitudes for the uniform random and foam-type aggregation microstructures as shown in Fig. 2. The background or imposed electric field amplitude (incident wave) was 1.000.

FIG. 4. Effective permittivities at 10 MHz for cluster and foam microstructures of solid particles (ε_1 = 8.5) in an air or vacuum matrix (ε_0 = 1.0), and plotted as a function of local particle volume fraction (volume fraction of particles in aggregated region). Average particle volume fraction remained constant at 0.30. Values are compared between the multipole (MP), Maxwell Garnett (MG), and Torquato (TQ) models.

FIG. 5. Effective permittivities at 10 MHz for cluster and foam microstructures of solid particles (ε_1 = 8.5) in an air or vacuum matrix (ε_0 = 1.0). Average particle volume fraction remained constant at 0.20. Values are compared between the multipole (MP) and Maxwell Garnett (MG) models.

FIG. 6. Effective permittivities at 10 MHz for cluster and foam microstructures of voids (ε_1 =

1.0) in a solid matrix (ε_0

8.5). Average void volume fraction remained constant at 0.20.

Values are compared between the multipole (MP) and Maxwell Garnett (MG) models.

FIG. 7. Effective permittivities as a function of frequency for the 0.20-volume fraction particle packs of solid particles ($\varepsilon_1 = 8.5$) in an air or vacuum matrix ($\varepsilon_0 = 1.0$). Trends are shown for the non-aggregated microstructure, the cluster microstructure at 0.5 local particle volume fraction, and the foam microstructure at 0.4 local particle volume fraction.

Figure 1

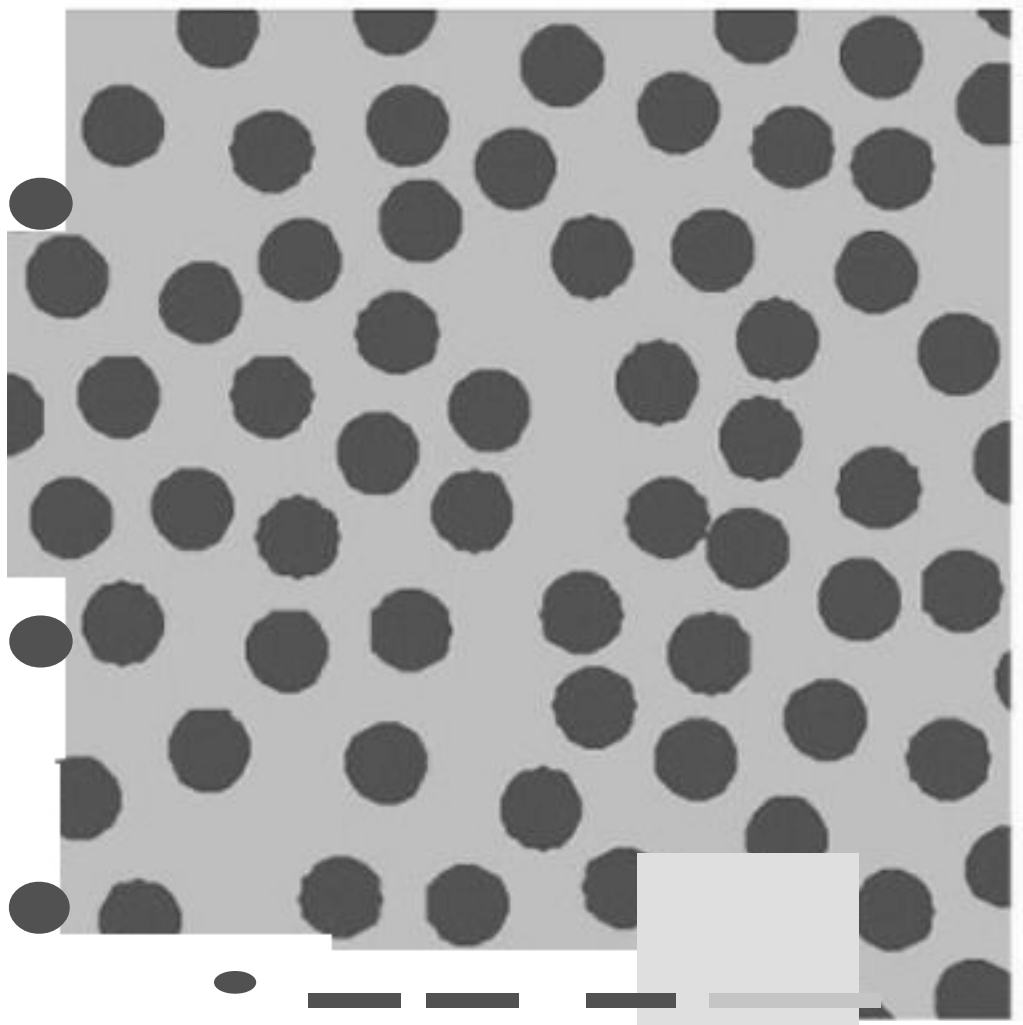

(a)

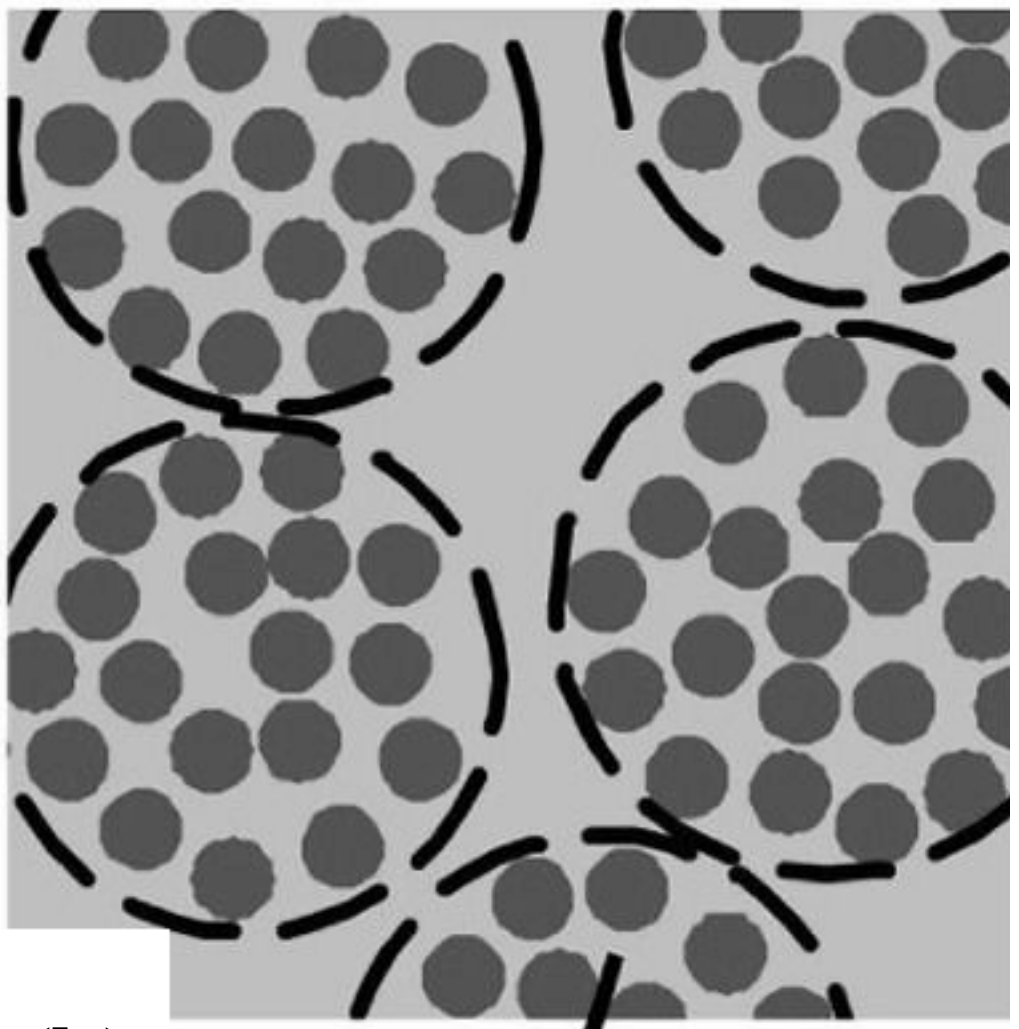

(b)

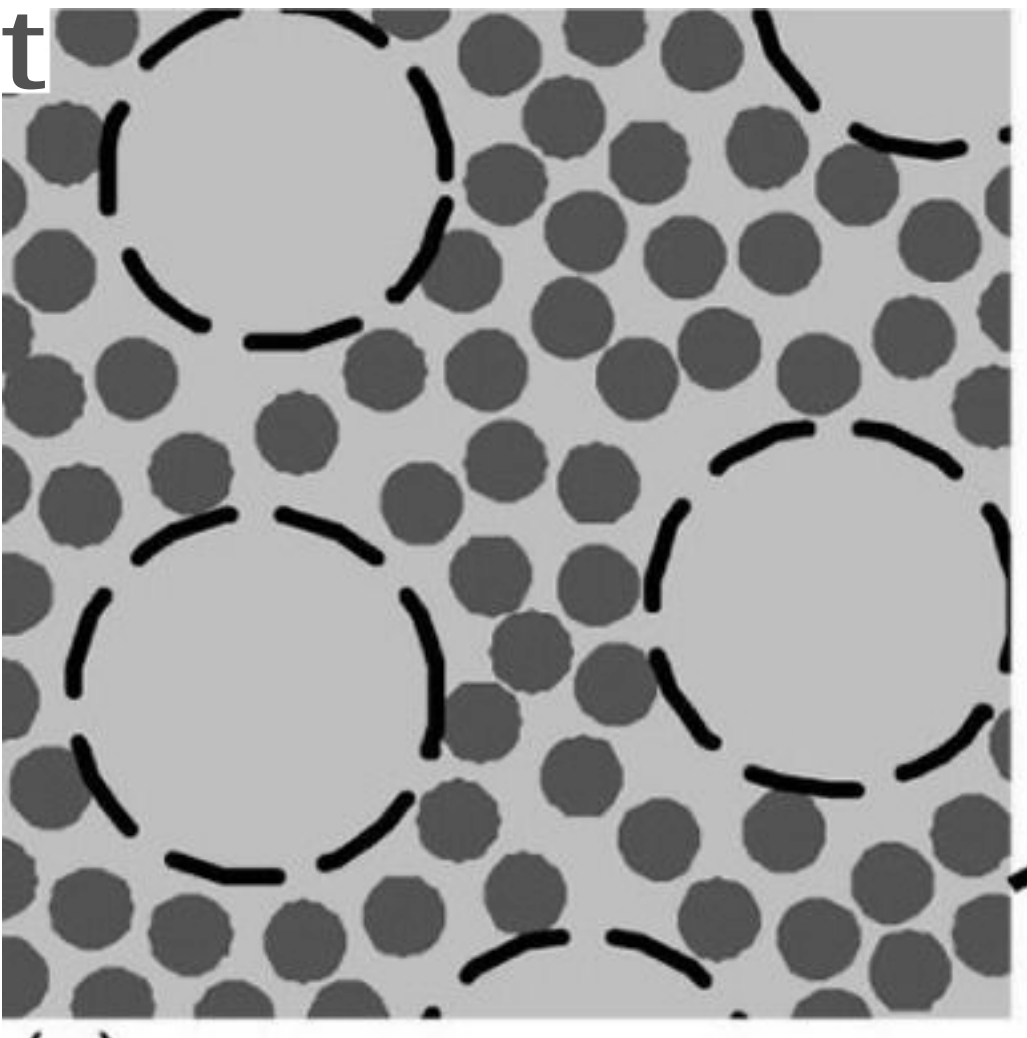

(c)

Quasi-particle

Quasi-matrix

Figure 2

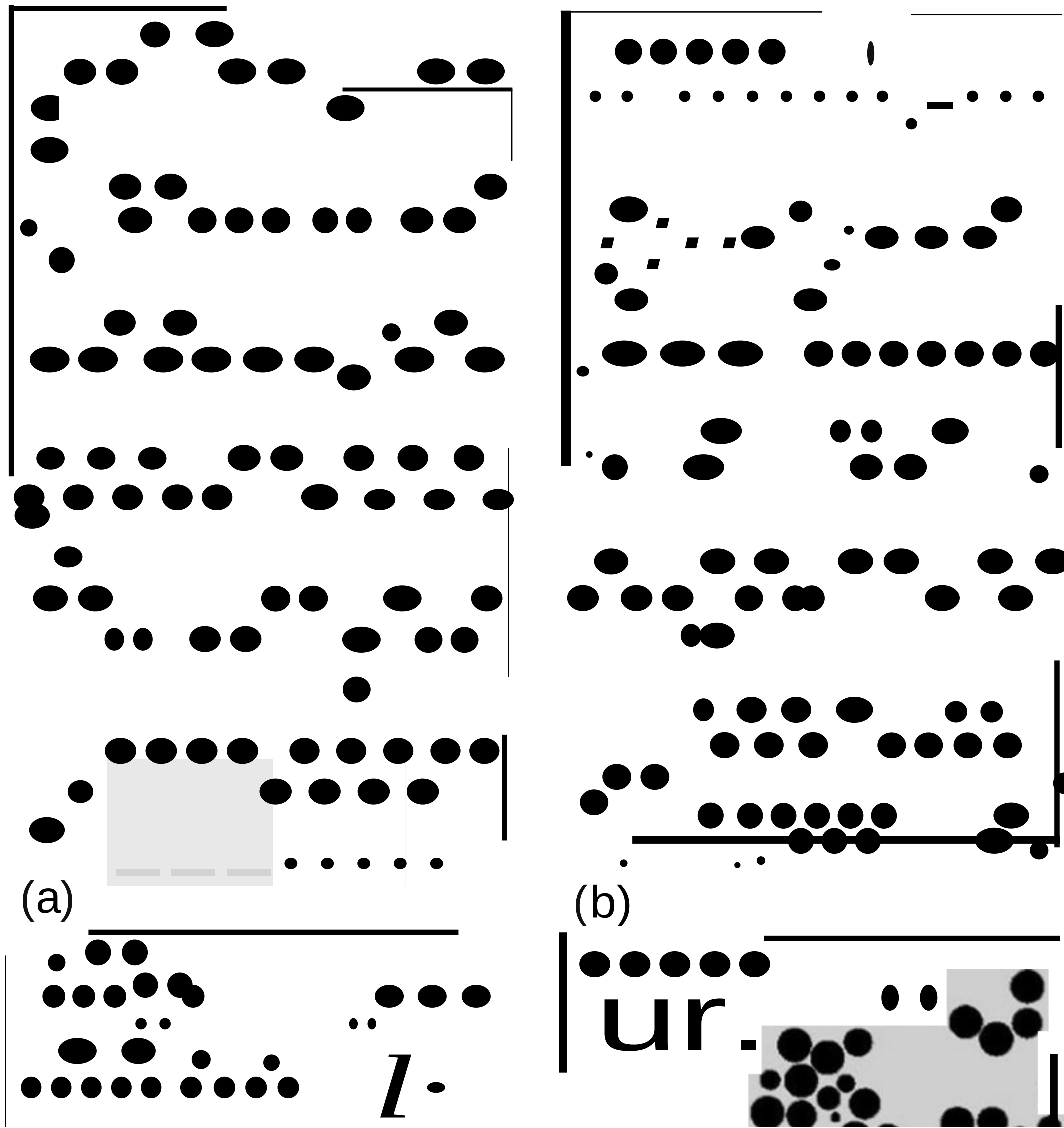

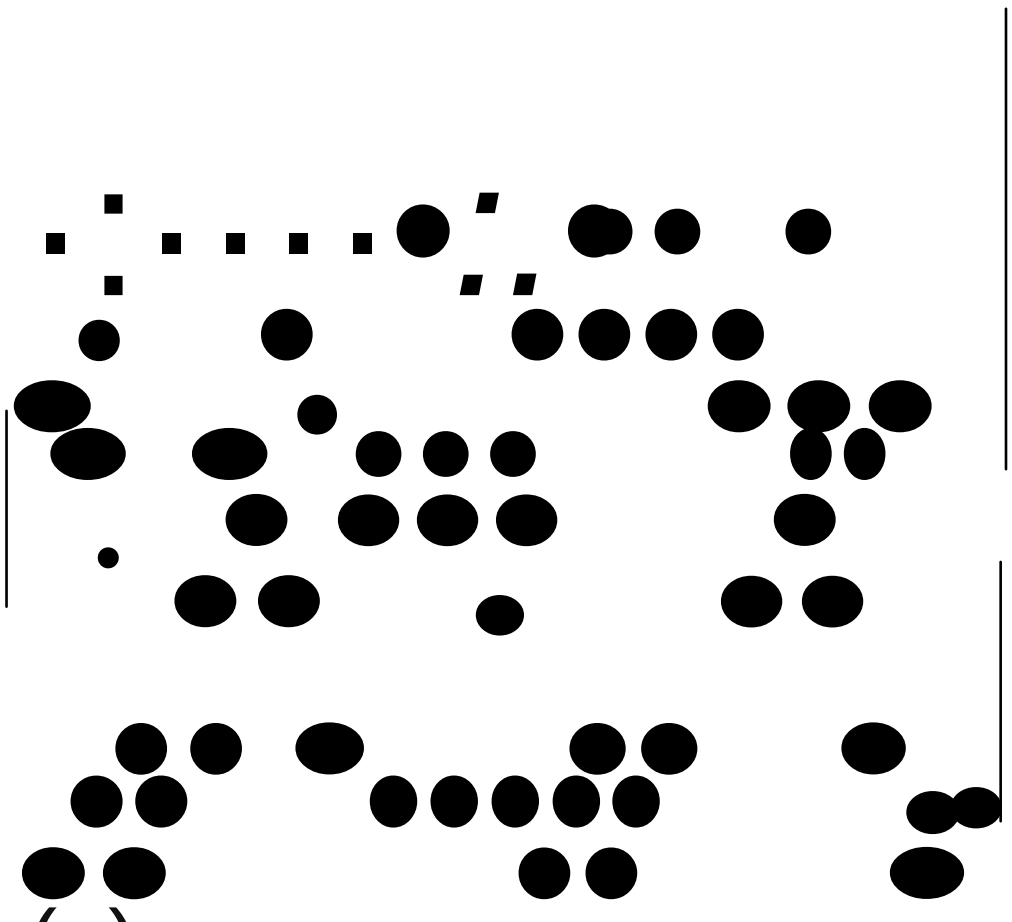

(c)

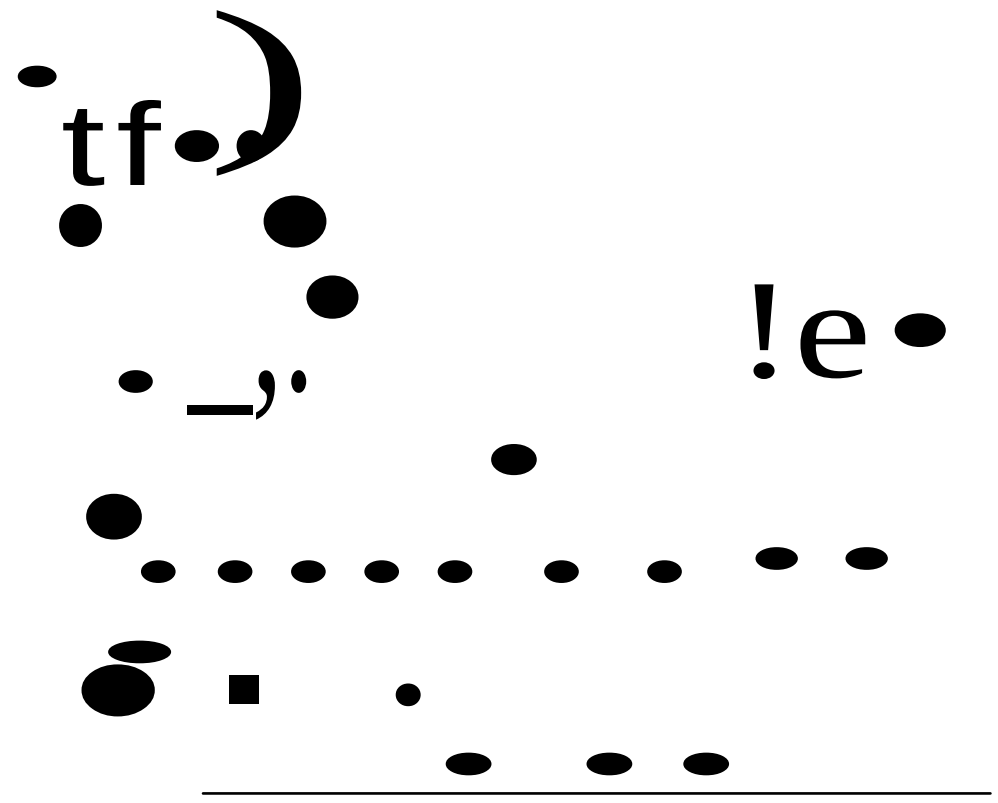

(d)

Figure 3

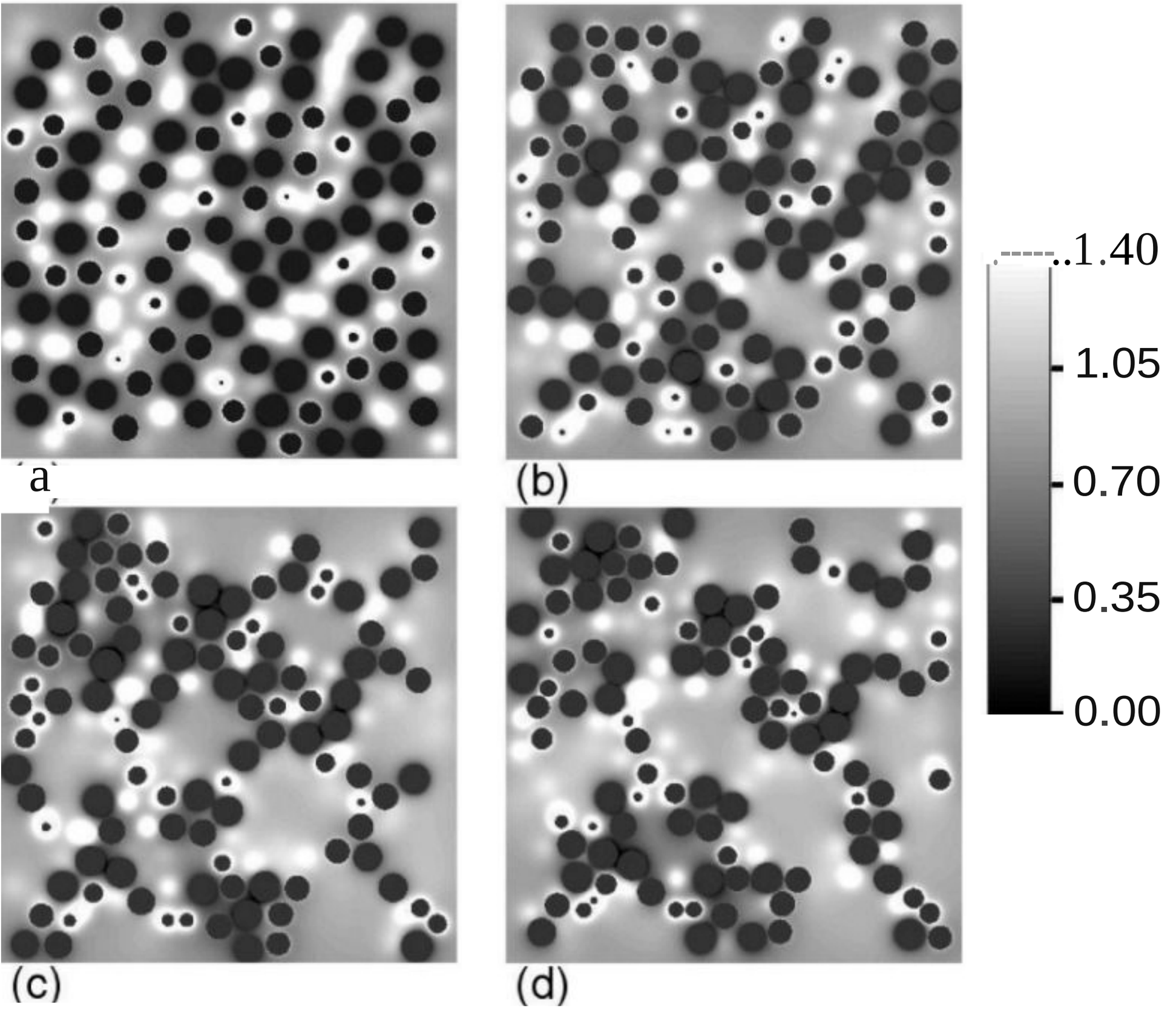

Figure 4

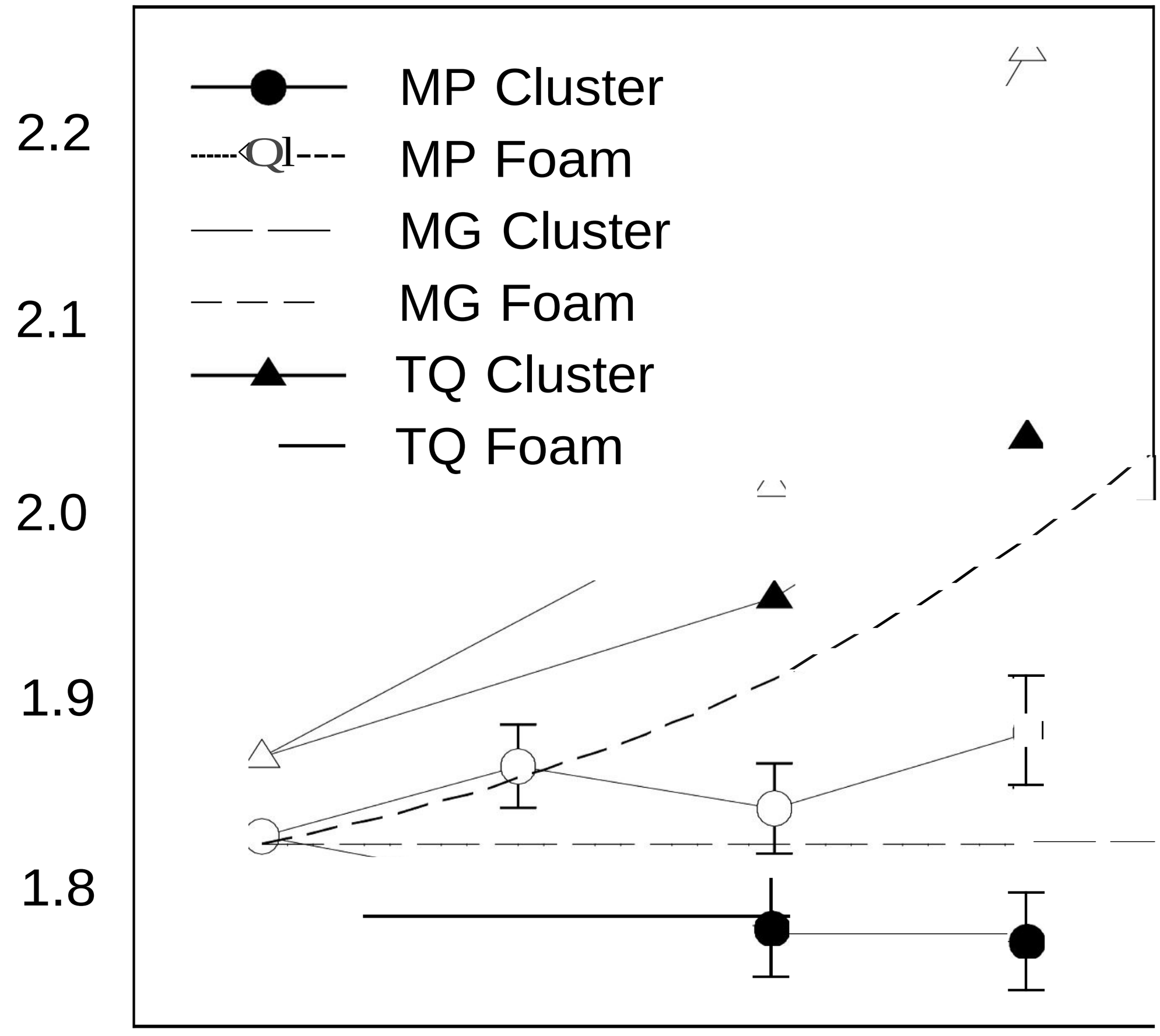
MP Cluster
MP Foam
MG Cluster
MG Foam
TQ Cluster
TQ Foam
2.2
2.1
2.0
1.9
1.8
0.3
0.4
0.5
0.6
Local Particle Vol. Fraction

Figure 5

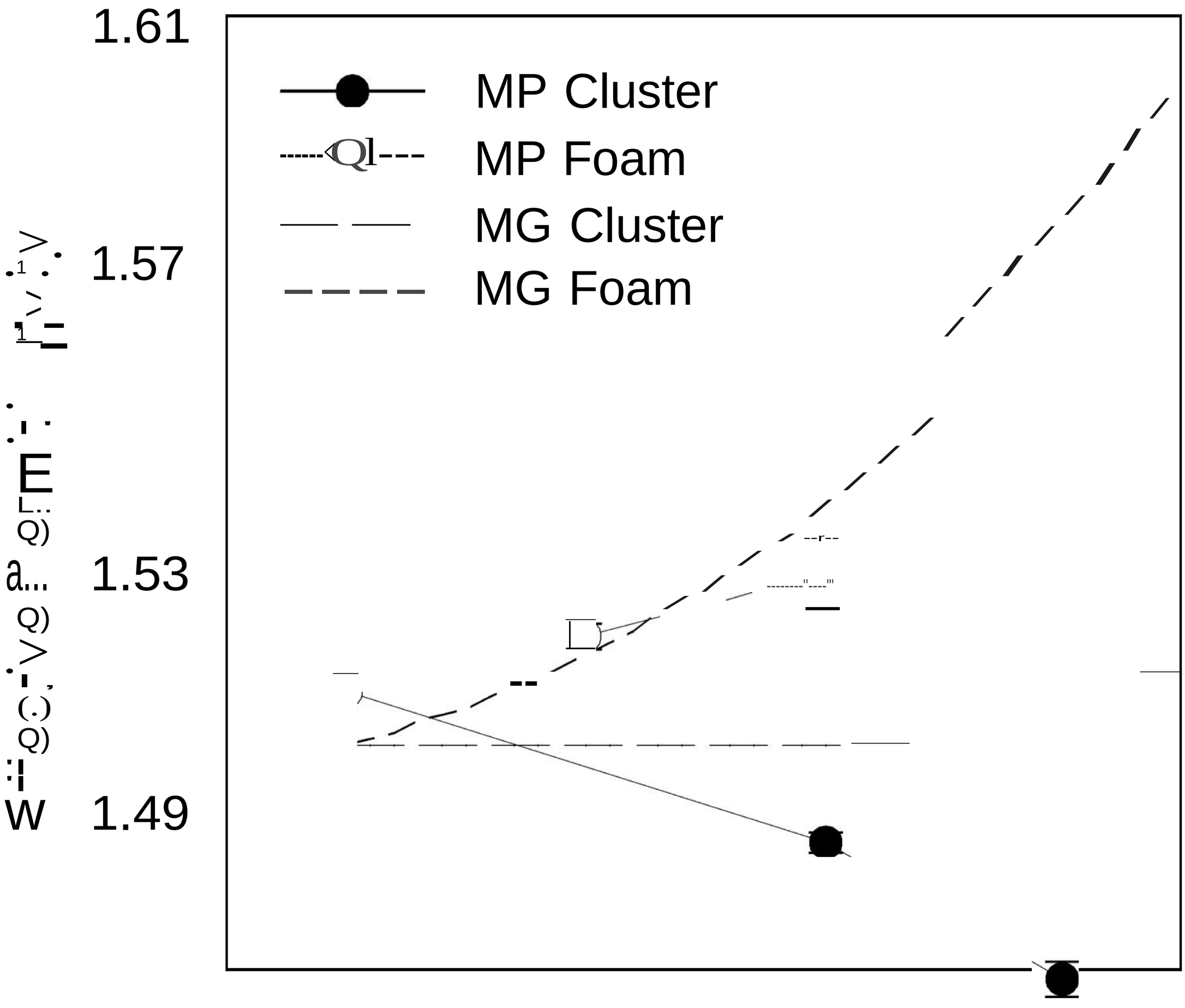
1.61
1.57
1.53
1.49
1.45
MP Cluster
MP Foam
MG Cluster
MG Foam
Local Particle Vol. Fraction

0.2 0.3 0.4 0.5

Local Particle Vol. Fraction

Figure 6

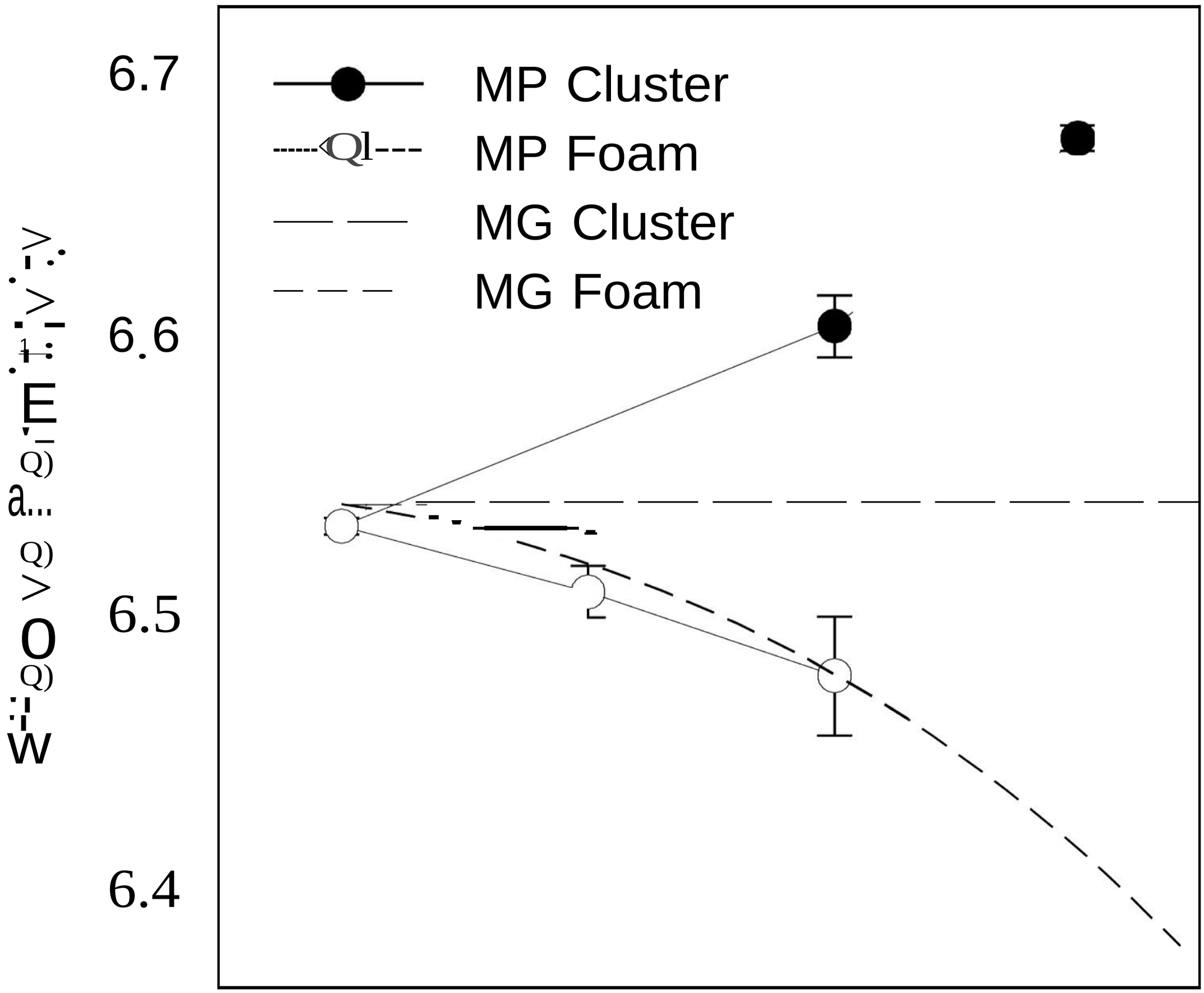
MP Cluster
MP Foam
MG Cluster
MG Foam
6.7
6.6
6.5
6.4
0.2
0.3
0.4
0.5
Local Particle Vol. Fraction

Figure 7

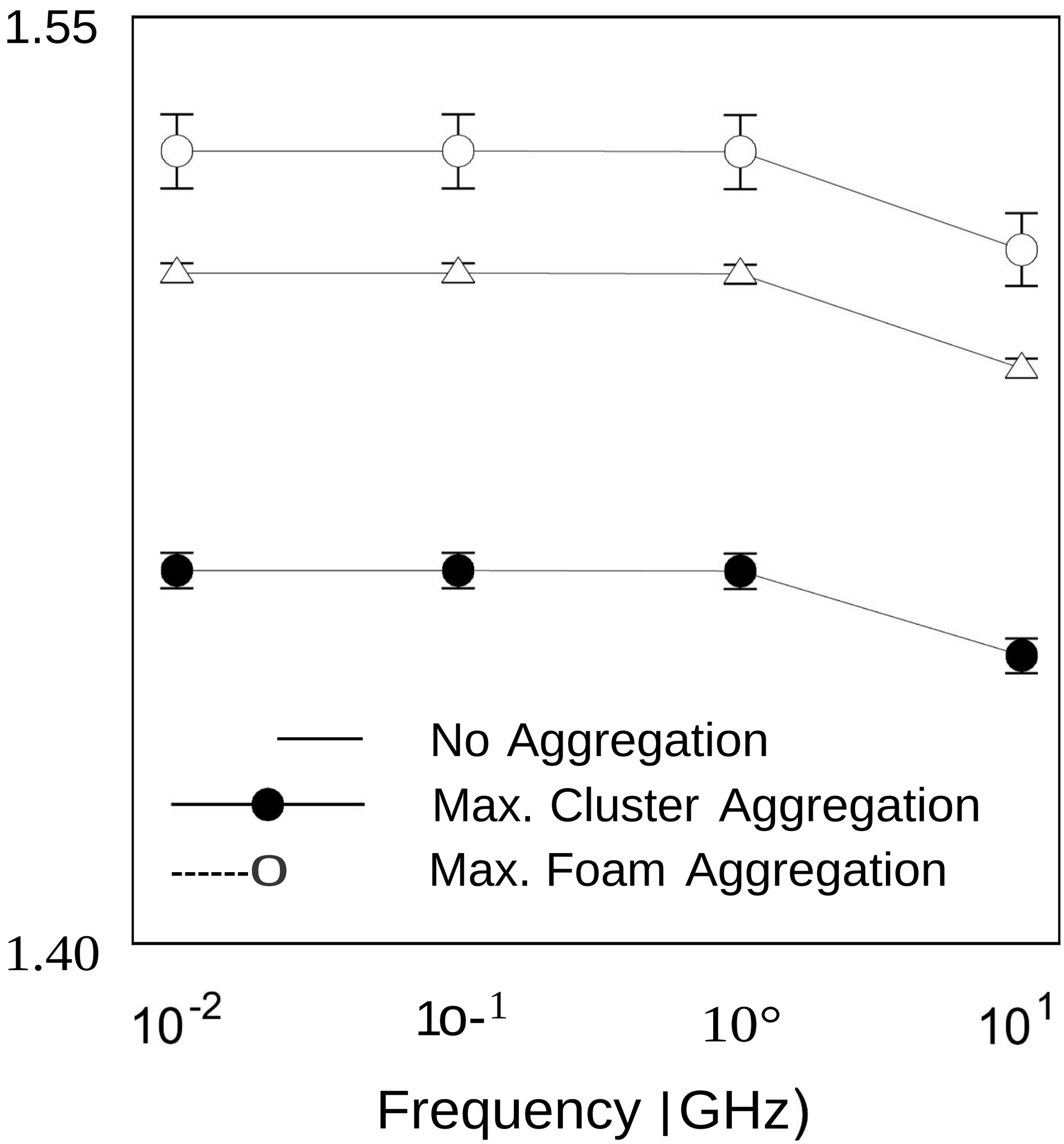
1.55
No Aggregation
Max. Cluster Aggregation
Max. Foam Aggregation
1.40
10-2
10-1
10°
101
Frequency |GHz)